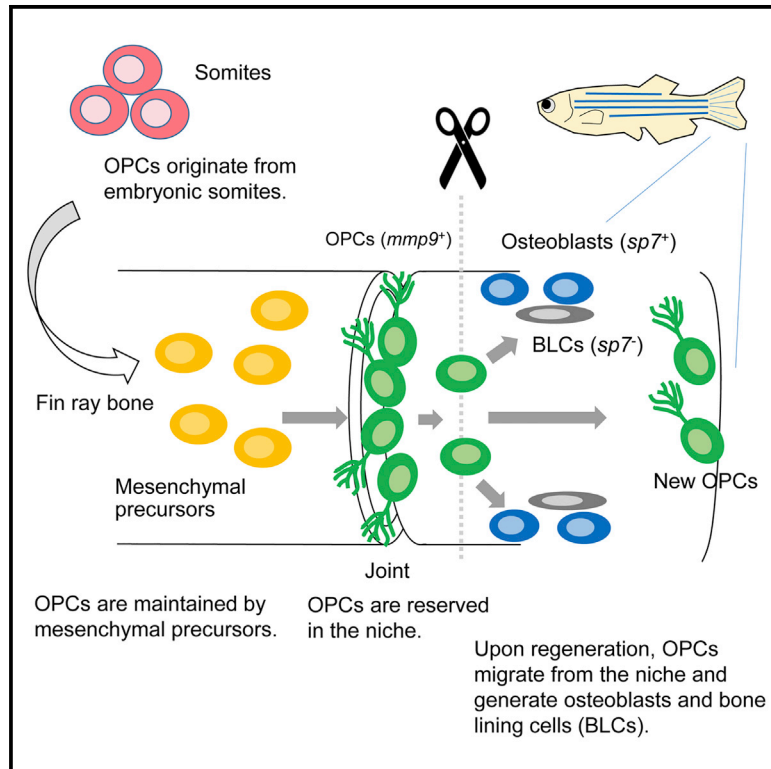# Osteoblast Production by Reserved Progenitor Cells in Zebrafish Bone Regeneration and Maintenance

Graphical Abstract

Authors

Kazunori Ando, Eri Shibata,
Stefan Hans, Michael Brand,
Atsushi Kawakami

Correspondence

atkawaka@bio.titech.ac.jp

In Brief

Ando et al. identify osteoblast progenitor cells (OPCs) in zebrafish and find that OPCs are derived from embryonic somites and are reserved in niches of bone-forming tissues while being replenished from mesenchymal precursors. OPCs migrate from the niches and generate osteoblasts during bone regeneration and maintenance in adult zebrafish.

Highlights

- Osteoblast progenitor cells (OPCs) are identified by cell-fate tracing in zebrafish

- OPCs are a complementary source of osteoblasts in regenerating fins after amputation

- OPCs are derived from embryonic somites and replenished from mesenchymal precursors

- OPCs also provide osteoblasts during homeostatic maintenance of fin ray bone

CellPress

Developmental Cell

Short Article

CellPress

Osteoblast Production by Reserved Progenitor Cells in Zebrafish Bone Regeneration and Maintenance

Kazunori Ando,[1] Eri Shibata,[1] Stefan Hans,[2] Michael Brand,[2] and Atsushi Kawakami[1,3,*]
[1]School of Life Science and Technology, Tokyo Institute of Technology, 4259 Nagatsuta, Midori-ku, Yokohama 226-8501, Japan
[2]Developmental Genetics, DFG-Center for Regenerative Therapies Dresden, Tatzberg 47/49, 01307 Dresden, Germany
[3]Lead Contact
*Correspondence: atkawaka@bio.titech.ac.jp
https://doi.org/10.1016/j.devcel.2017.10.015

SUMMARY

Mammals cannot re-form heavily damaged bones as in large fracture gaps, whereas zebrafish efficiently regenerate bones even after amputation of appendages. However, the source of osteoblasts that mediate appendage regeneration is controversial. Several studies in zebrafish have shown that osteoblasts are generated by dedifferentiation of existing osteoblasts at injured sites, but other observations suggest that *de novo* production of osteoblasts also occurs. In this study, we found from cell-lineage tracing and ablation experiments that a group of cells reserved in niches serves as osteoblast progenitor cells (OPCs) and has a significant role in fin ray regeneration. Besides regeneration, OPCs also supply osteoblasts for normal bone maintenance. We further showed that OPCs are derived from embryonic somites, as is the case with embryonic osteoblasts, and are replenished from mesenchymal precursors in adult zebrafish. Our findings reveal that reserved progenitors are a significant and complementary source of osteoblasts for zebrafish bone regeneration.

INTRODUCTION

Calcified tissues are crucial for supporting the body structures of vertebrates. After amputation of an appendage in urodeles and teleost fish, new cartilage or bone structures of appropriate sizes and shapes emerge from the blastema, a mass of proliferative cells (Brockes and Kumar, 2005; Kawakami, 2010). Defining the cellular sources of regenerated skeletal elements has been one of the most important objectives in increasing our understanding of the mechanism of appendage regeneration (Poss, 2010; Tanaka and Reddien, 2011; Yoshinari and Kawakami, 2011).

A recent study in axolotl limb regeneration by Kragl et al. (2009) investigated the contributions of tissues constitutively expressing a fluorescent reporter protein grafted from transgenic axolotls. The study suggested a model in which cartilage cells predominantly contribute to their own tissue during axolotl limb

regeneration, while one or more cell populations within the dermis also have the potential to form cartilage.

In teleost fish, fins contain an array of radially arranged and segmented fin rays lined by osteoblasts. Several recent studies in zebrafish investigated the cellular source of regenerated osteoblasts by genetic lineage tracing during fin regeneration and suggested that osteoblasts are generated by dedifferentiation, proliferation, and migration of lineage-restricted stump osteoblasts (Knopf et al., 2011; Tu and Johnson, 2011; Sousa et al., 2011; Stewart and Stankunas, 2012).

On the other hand, Singh et al. (2012) demonstrated that zebrafish fins that were depleted of virtually all skeletal osteoblasts by genetic ablation methods restored the osteoblasts and regenerated as normal within 2 weeks, indicating that *de novo* osteoblast production also occurs. However, the identity and nature of such osteoblast-producing cells, their normal contribution to regeneration, and their role in non-regenerating skeletal tissues have not yet been revealed.

In this study, we report that a population of cells expressing *matrix metalloproteinase 9* (*mmp9*) serves as osteoblast progenitor cells (OPCs) during regeneration and maintenance of calcified tissues in zebrafish. We also show that OPCs are derived from embryonic somites and replenished from *mmp9⁻* mesenchymal precursor cells in adult zebrafish. An array of precursor pools such as the OPCs and their mesenchymal precursors is thought to be an important regulatory mechanism that reinforces and ensures robust bone regeneration and maintenance.

RESULTS AND DISCUSSION

Recruitment of *mmp9⁺* Cells from Fin Ray Joints to Regenerates

We previously identified the *mmp9* gene as a highly upregulated gene during fin and fin fold regeneration in zebrafish (Yoshinari et al., 2009). To understand the *mmp9⁺* cell identity and its role during regeneration, we generated bacterial artificial chromosome (BAC) transgenic zebrafish (*Tg*) that expressed the *EGFP* gene under regulation of the *mmp9* gene (Figure S1A). The *Tg* displayed a unique EGFP expression before regeneration at fin ray joints (Figures S1B and S1C). Besides that in fins, EGFP fluorescence was also observed in mineralized tissues such as those of the cranial bones, gills, vertebral arches, and scales (Figure S1D). Intriguingly, when the caudal fin of the *Tg* was
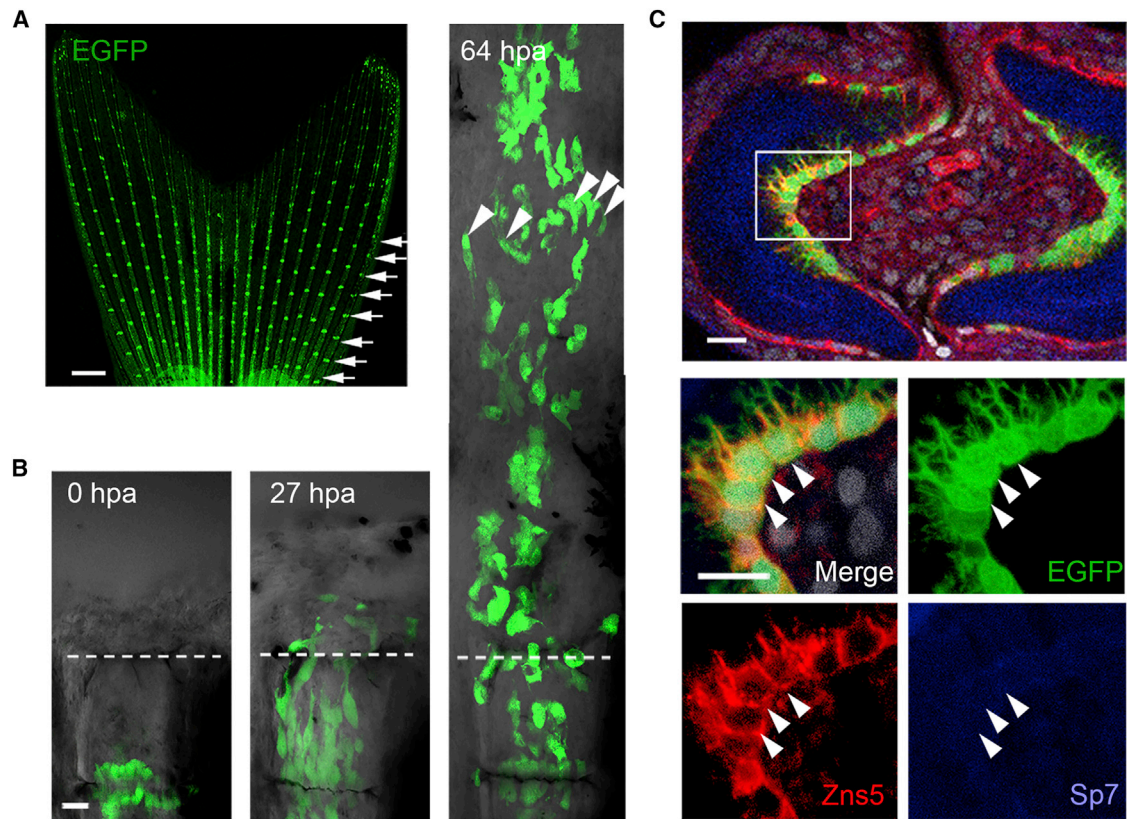
Figure 1. *mmp9*[+] Cells in Fin Ray Joints Migrate to Contribute to Tissue Regeneration

(A) Labeling of *mmp9*^{+} joint cells by Cre-*loxP* recombination. Treatment of *Tg(mmp9:CreERt2; Olactb:loxP-dsred2-loxP-egfp)* with TAM induced the expression of EGFP in cells of the joints (arrows). Scale bar, 500 μm.

(B) Tracking of EGFP-labeled cells during regeneration. The marked cells migrated distally to become cells within the regenerated tissue including cells in the regenerating joint (arrowheads). Dashed lines, amputation sites. Scale bar, 10 μm.

(C) Zns5 and Sp7 antibody staining of a cross-section through the joint of Cre-labeled *Tg*. *mmp9*-expressing joint cells have a characteristic cell shape with dendritic projections and are positive for Zns5 (cell-surface labeling), but not Sp7. The absence of *sp7* expression in the *mmp9*^{+} joint cells is also seen in the *Tg(sp7:mcherry)* (Figure 3F). Nuclei, TO-RPO-3. Arrowheads, representative cells that are positive for EGFP and Zns5, but not Sp7. Scale bar, 10 μm.

amputated to induce regeneration, time-lapse observation suggested that EGFP^{+} cells migrated from the nearest joints, reached the plane of amputation at 22 hr post amputation (hpa), and became *mmp9*^{+} cells within the regenerating tissue (Figures S1B, S1E, and S1F). A similar emergence of *mmp9*^{+} cells in response to tissue injury was observed during bone fracture healing and scale regeneration (Figures S1G and S1H).

To further confirm the migration of *mmp9*^{+} cells from joints to regenerates, we generated another BAC *Tg* line that expressed the Cre recombinase (CreERt2) under control of the *mmp9* gene (Figure S1A) and tracked the fate of *mmp9*^{+} joint cells. In the double *Tg(mmp9:CreERt2; Olactb:loxP-dsred2-loxP-egfp)*, almost no EGFP^{+} cells were observed in the absence of 4-hydroxy tamoxifen (TAM) in embryos, larvae, or regenerating larval fin fold. In adult caudal fin, a few EGFP^{+} cells appeared over time (Figure S1I). However, we did not detect newly induced EGFP^{+} cells during fin regeneration in the absence of TAM. When recombination was induced with TAM, the joint cells became EGFP[+] within 3 days in a pattern similar to that of *Tg(mmp9:egfp)* (Figure 1A). Because TAM-independent recombinations were far fewer than those of TAM-induced ones, it

was assumed that TAM-independent recombination does not affect the results of cell-fate tracing. After at least 2 days of TAM washout, fin amputation and cell-fate analysis were performed. The Cre-labeled cells migrated out from the joints and contributed to cells in the regenerated tissue (Figure 1B), confirming that *mmp9*^{+} joint cells migrate in response to tissue injury and become cells within regenerated tissue.

mmp9[+] Cells in the Fin Ray Joint Are Osteoblast Progenitor Cells

It has been suggested that *mmp9* is expressed in osteoclasts (Sharif et al., 2014). We examined tartrate-resistant acid phosphatase (TRAP) stains of the osteoclasts in *Tg(mmp9:egfp)*; however, the results indicated that most TRAP^{+} cells did not overlap with EGFP^{+} cells (Figure S2A), suggesting that most *mmp9*^{+} cells were not osteoclasts.

Unlike differentiating osteoblasts or osteocytes, *mmp9*^{+} cells in fin ray joints have characteristic dendritic projections (Figure 1C) and were positive for Zns5, an uncharacterized cell-surface antigen that helps identify osteoblasts (Johnson and Weston, 1995). This suggests that *mmp9*^{+} joint cells have
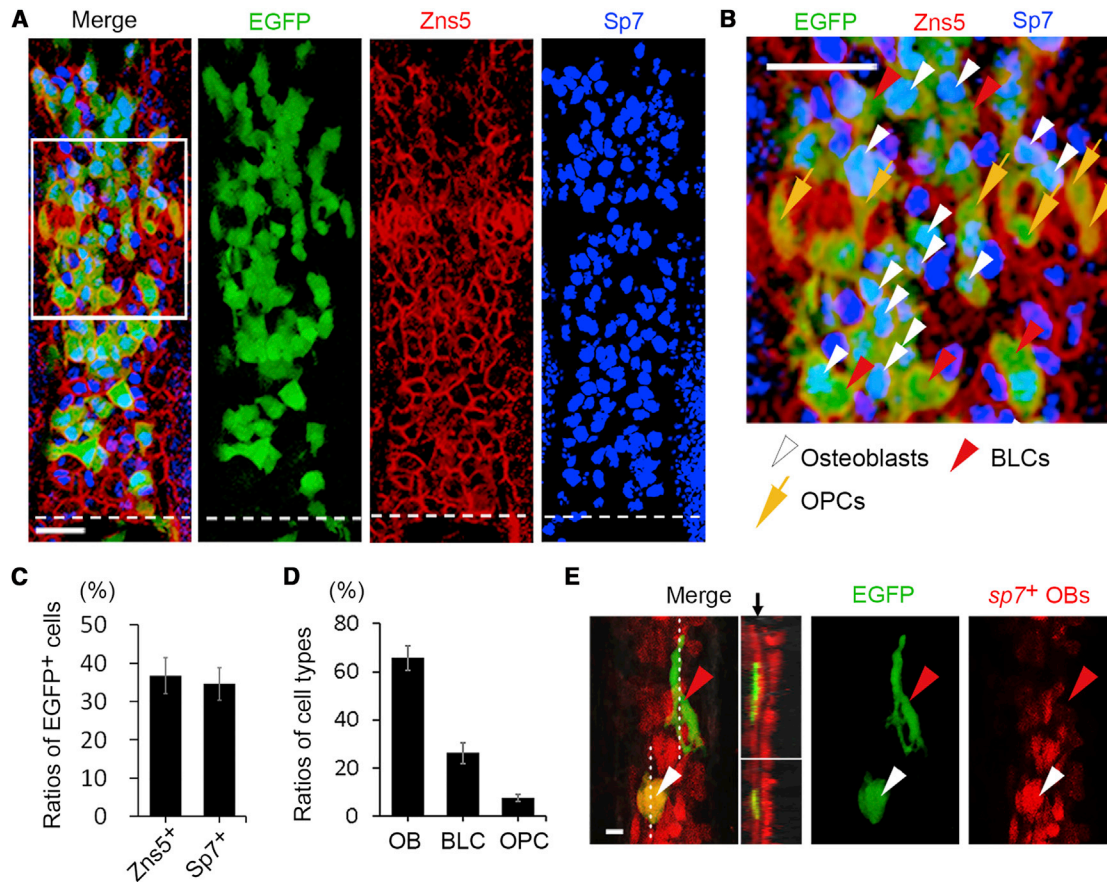
Figure 2. *mmp9*+ Cells Are the Osteoblast Progenitor Cells during Fin Regeneration

(A) Confocal image of a longitudinal section of Cre-labeled *Tg* fin at 2 days post amputation (dpa) that were stained with Sp7, Zns5, and EGFP antibodies. Sp7 proteins and Zns5 antigens are localized in the nucleus and on the cell surface, respectively. Respective positive cells were also confirmed by nuclear staining with TO-PRO-3 (not shown). Many of the migrated *mmp9*+ joint cells became Sp7+ or Zns5+ cells in the regenerates. Dashed lines, amputation sites. Scale bar, 20 μm.

(B) Magnification of boxed area in (A). Progenies of *mmp9*+ joint cells produced Sp7+ osteoblasts (white arrowheads), Sp7− BLCs (red arrowheads), or regenerated OPCs (yellow arrows). Scale bar, 20 μm.

(C) Quantification of joint-derived (EGFP+) cells among Sp7+ or Zns5+ cells. Cells were counted on confocal optical sections in area distal to the amputation plate. n = 20 optical sections (different fin rays, total 5 fish). Error bars indicate mean ± SEM.

(D) Ratios of contribution of joint-derived cells to osteoblasts (OBs), BLCs, or OPCs in the regenerated tissue. n = 15 fin rays (total 5 fish). Error bars indicate mean ± SEM. Cell count was performed on confocal z-stack images to confirm respective antibody staining in individual cells. OPCs and BLCs, which are Sp7−, were distinguished by their cell morphologies and tissue localization: OPCs, elongated shape along proximal-distal axis with localization in fin ray joints; BLCs, a flattened irregular shape with non-joint distribution.

(E) Confocal image of a regenerating Cre-labeled *Tg* fin at 4 dpa, which also carries the *sp7:mcherry* transgene. Dashed lines indicate planes of optical sections shown on the right. Arrow, growing bone matrix; red arrowheads, BLCs; white arrowheads, OBs. Scale bar, 10 μm.

features characteristic of osteoblast-lineage cells. However, they were not positive for Sp7, a zinc-finger transcription factor whose expression is first seen during intermediate stages of osteoblast differentiation (Li et al., 2009; Renn and Winkler, 2009) (Figure 1C).

In contrast to *mmp9*+ joint cells, many Cre-labeled cells that migrated to the regenerated tissue became positive for both Sp7 and Zns5 (Figures 2A, 2B, and S2B–S2D, white arrowheads), indicating that *mmp9*+ joint cells differentiated into osteoblasts; therefore, *mmp9*+ joint cells serve as osteoblast progenitor cells (OPCs) during regeneration. Considering that the efficacy of Cre recombination is less than 100%, it can be concluded that at least 40% of the osteoblasts within the regen-

erated tissue are derived from *mmp9*+ joint cells (Figures 2C and S2D). Additionally, OPCs gave rise to Sp7− cells within the regenerated tissue that were not directly in contact with the bone surface and had irregular and flat shapes (Figures 2D and 2E). As they exhibit such localization and lack of Sp7 expression, they may correspond to the bone lining cells (BLCs), which were thought to retain the potential to become osteoblasts in a study of a mouse model (Matic et al., 2016).

Besides differentiation into osteoblasts and BLCs, the migrated *mmp9*+ cells also gave rise to regenerated joint cells (Figure 1B, arrowheads). Similar to the *mmp9*+ joint cells, they did not express Sp7 (Figures 2A, 2B, S2B, and S2C, yellow arrows). Intriguingly, a row of newly regenerated joint cells

CellPress

initially expressed the pre-osteoblast marker Runx2 (Dallas et al., 2013), but not Sp7 (Figure S2E, upper panels, yellow arrowheads). As regeneration proceeded, this initially formed OPCs lost Runx2 expression and became Runx2⁻/Sp7⁻ joint cells when the next row of OPCs were formed (Figure S2E, lower panels, yellow arrowheads), and in turn newly regenerated joint cells expressed Runx2 (Figure S2E, lower panels, white arrowheads), indicating that *mmp9*⁺ joint cells renew themselves by way of a transient pre-osteoblastic state. Furthermore, over 90% of the joint-derived cells incorporated EdU (5-ethynyl-2′-deoxyuridine) between 24 and 48 hpa irrespective of their fates as either osteoblasts or new OPCs (Figures S2F and S2G).

Significant Contribution of OPCs to Fin Ray Bone Regeneration
To assess the significance of OPCs in bone regeneration, we performed OPC ablation experiments using a newly generated BAC *Tg* line, which expressed the *egfp-nfsB* fusion gene under *mmp9* regulation (Figure S1A). The *nfsB* gene encodes the bacterial nitroreductase, an enzyme that kills *nfsB*-expressing cells only when a small molecule, metronidazole (Mtz), is added to fish water (Pisharath et al., 2007). In the *Tg*, *mmp9*⁺ cells including myeloid cells (Figure S1E, arrows) were eliminated within 48 hr after addition of Mtz (Figure 3A). After Mtz treatment, regeneration of calcified fin ray tissue and the numbers of Sp7⁺ and Zns5⁺ cells in the regenerated tissue were significantly reduced in the *Tg* (Figures 3B–3E); however, overall tissue regeneration and growth were not affected (Figures S3A–S3C). Consistently, the expressions of the regeneration-induced genes *fibronectin* (*fn*) *1b* in the epidermis (Yoshinari et al., 2009) and *msxc* in the blastema (Akimenko et al., 1995) were unaffected by OPC ablation (Figure S3D). Thus, the results indicated that OPCs localized in the fin ray joints are a *de novo* and significant source of osteoblasts for bone regeneration. This is consistent with previous observations by Singh et al. (2012) and explains why amputated fins depleted of pre-existing osteoblasts, which dedifferentiate to generate proliferative osteoblasts, regenerated new fin ray structures as normal.

Mesenchymal Precursor Cells Replenish OPCs
Intriguingly, when Mtz was removed after OPC ablation, OPCs at the joint re-formed within 4 days (Figure S3E), suggesting that OPCs are replenished by *mmp9*⁻ precursor cells. To examine the possibility that the re-formed OPCs are derived from osteoblasts, we used double *Tg*(*sp7:mcherry*; *mmp9:egfp-nfsB*) and tested whether re-formed OPCs (EGFP⁺) were derived from mCherry-expressing osteoblasts. However, we only detected EGFP⁺/mCherry⁻ OPCs (Figure 3F, arrowheads), suggesting that the osteoblasts did not dedifferentiate to form OPCs.

Next, we tested an alternative possibility that OPCs were replenished by *mmp9*⁻ mesenchymal cells around fin joints. To test this idea, we performed blastema transplantations (Yoshinari et al., 2012; Shibata et al., 2016, 2017) and introduced mesenchymal cells from double *Tg*(*mmp9:egfp*; *Olactb:loxP-dsred2-loxP-egfp*), which ubiquitously and constitutively expresses Discosoma red fluorescent protein 2 (DsRed2) (Yoshinari et al., 2012), into the host *Tg*(*mmp9:egfp-nfsB*). After transplantation, over 95% of transplanted blastema cells give

rise to mesenchymal cells in fin rays, but not to osteoblasts (Shibata et al., 2016). If donor mesenchymal cells became OPCs after ablation, they became DsRed2⁺/EGFP⁺ (Figure 3G). When host OPCs were ablated in the continuous presence of Mtz, DsRed2⁺ OPCs derived from transplanted mesenchymal cells appeared in host joints (Figures 3H and S3F, arrowheads). Although fin ray mesenchymal cells derived from transplanted blastema could be a heterogeneous cell population, the result suggests that OPCs can be replenished from precursor cells that exist in fin rays.

Lineage and Embryonic Origin of OPCs
To examine OPC cell lineages during development and growth, we performed cell-fate tracing during the early stage of fin growth. When 2–3 rows of OPCs were formed at 25 days post fertilization (dpf), we labeled them using a Cre-*loxP* recombination. After 23 days, progenies of the early-formed OPCs contributed neither to joints formed later nor to osteoblasts in the distal fin region (Figure 4A), indicating that new OPCs are not generated by pre-existing OPCs but by other *mmp9*⁻ cells during development and growth.

We further sought to identify the developmental origin of OPCs. To this end, we adopted the somite transplantation approach, which is an excellent method for tracing somite-derived cells without a detectable level of contamination of non-somite cells (Shimada et al., 2013). A previous study in medaka fish has shown that fin osteoblasts and scale mineral-forming cells originate from somites (Shimada et al., 2013). We postulated that OPCs are also derived from somites, and transplanted embryonic somites from double *Tg*(*mmp9:egfp*; *Olactb:loxP-dsred2-loxP-egfp*) into wild-type (WT) hosts (Figure 4B). As in the medaka fish, cells derived from somites gave rise to osteoblasts in fin rays and scales (Figures 4C and S4C). Importantly, the transplanted somite cells also differentiated into the EGFP⁺ OPCs in fin ray joints (Figures 4C and S4D) and scales (Figure S4C) in a reproducible fashion, strongly suggesting that OPCs develop from embryonic somites, as is the case with embryonic osteoblasts.

Role of OPCs during Fin Growth and Maintenance
So far, we revealed the significant role of OPCs during fin ray bone regeneration. We now further investigated the role of OPCs during fin growth and maintenance. OPC ablation was performed by repeated treatment with Mtz from 20 to 28 dpf, during which period rapid fin growth occurred (Figure S4E), but no significant difference in calcified bone formation nor osteoblast number was detected in either the *Tg* or WT (Figures S4F–S4I). We further examined the role of OPCs in osteoblast maintenance in adult zebrafish, in which ablation by repeated treatment with Mtz started from 3 months of age and continued for 40 days (Figure S4J). However, there was little effect on osteoblast number and calcified tissue formation (Figures S4K–S4N). Because the emergence of EGFP⁺ cells was detected in neither cell ablation experiment throughout Mtz treatment, it is unlikely that rapidly regenerating OPCs produced osteoblasts. This may suggest that both *mmp9*⁺ OPCs and *mmp9*⁻ precursors give rise to new osteoblasts during homeostasis, with the *mmp9*-precursors sufficient to maintain normal homeostasis in the absence of OPCs.
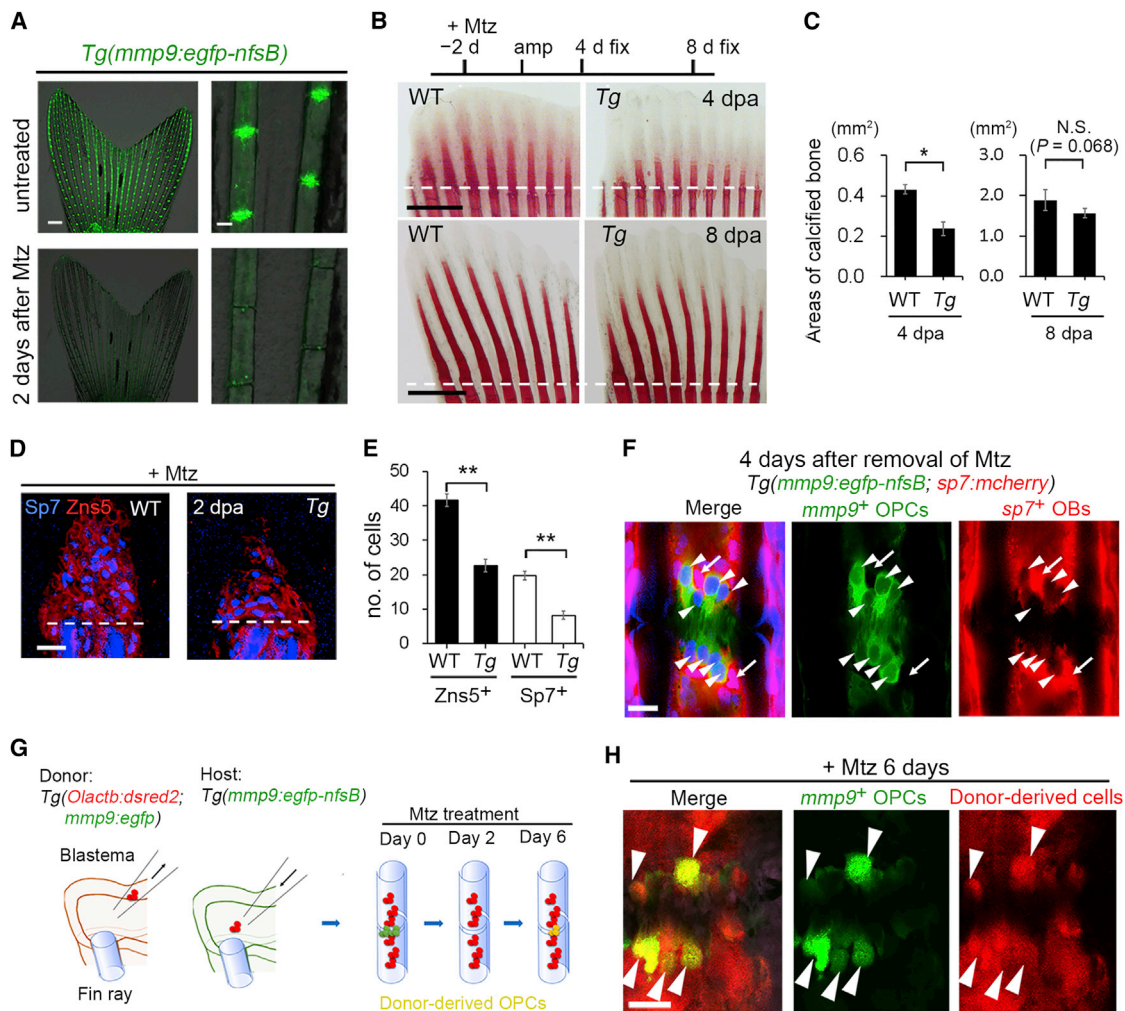
Figure 3. OPCs Replenished from Mesenchymal Precursors Are Significant Contributors to Bone Regeneration

(A) A representative example of OPC ablation. Effective ablation of the OPCs occurs with 5 mM Mtz treatment for 2 days. Scale bars, 500 μm (left panel) and 50 μm (right panel).

(B) Alizarin red S staining of regenerating WT and nfsB-expressing Tg fins treated with Mtz. Dashed lines indicate fin amputation sites. Scale bars, 500 μm.

(C) Quantification of calcified areas in (B). A significant decrease of calcified tissue was observed when OPCs were ablated. Error bars indicate mean ± SEM. *p < 0.01, Student's two-tailed t test; n = 5 fins. N.S., not significant.

(D) Detection of Zns5 and Sp7 in WT and OPC-ablated Tg regenerates. Dashed lines indicate fin amputation sites. Nuclei were counterstained with DAPI. Scale bars, 10 μm.

(E) Quantification of (D). The numbers of Zns5^{+} and Sp7^{+} cells, respectively, were significantly decreased by OPC ablation. Error bars indicate mean ± SEM. **p < 0.001, Student's two-tailed t test; n = 6 confocal optical sections from different fin rays (total 5 fish).

(F) Replenishment of OPCs from non-osteoblast precursors. In double Tg(sp7:mcherry; mmp9:egfp-nfsB), re-formed OPCs (arrowheads) after ablation were not mCherry[+] (n = 15 of 15 joints from total 5 fish), indicating that re-formed OPCs were not derived from mCherry[+] osteoblasts. Arrows point to nearby osteoblasts. Nuclei, DAPI. Scale bar, 10 μm.

(G) Procedure of mesenchymal cell transplantation and host OPC ablation. Olactb:dsRed2 refers to Olactb:loxP-dsred2-loxP-egfp. Donor blastema was transplanted into the host blastema region (Shibata et al., 2016). Most of the transplanted cells contribute to mesenchymal cells. Eight days after transplantation, host OPCs were ablated with 5 mM Mtz to see whether or not the re-formed joint cells (EGFP[+]) were derived from DsRed2^{+} mesenchymal cells.

(H) Emergence of OPCs from mesenchymal cells. Arrowheads point to re-formed OPCs derived from DsRed2^{+} mesenchyme. n = 24 fin ray joints from total 5 fish. Scale bar, 10 μm.

To further explore the normal role of OPCs in non-regenerating tissues, we performed long-term cell-fate tracing of OPCs. The Cre-loxP recombination of OPCs was performed at 4 months of age and fates were tracked over 114 days. The progenies of labeled OPCs were gradually distributed over the fin rays (Figure 4D). These cells consisted of Sp7^{+} osteoblasts and Sp7^{−} BLCs (Figures 4E and 4F). On the other hand, EGFP[+] osteoblasts or BLCs were not observed in fin rays of the double Tg(mmp9:creERt2; Olactb:loxP-dsred2-loxP-egfp) that were not treated with TAM (Figure S1I). These observations suggest that OPCs in fin ray joints produce osteoblasts and BLCs as normal for homeostatic maintenance of adult fin rays.
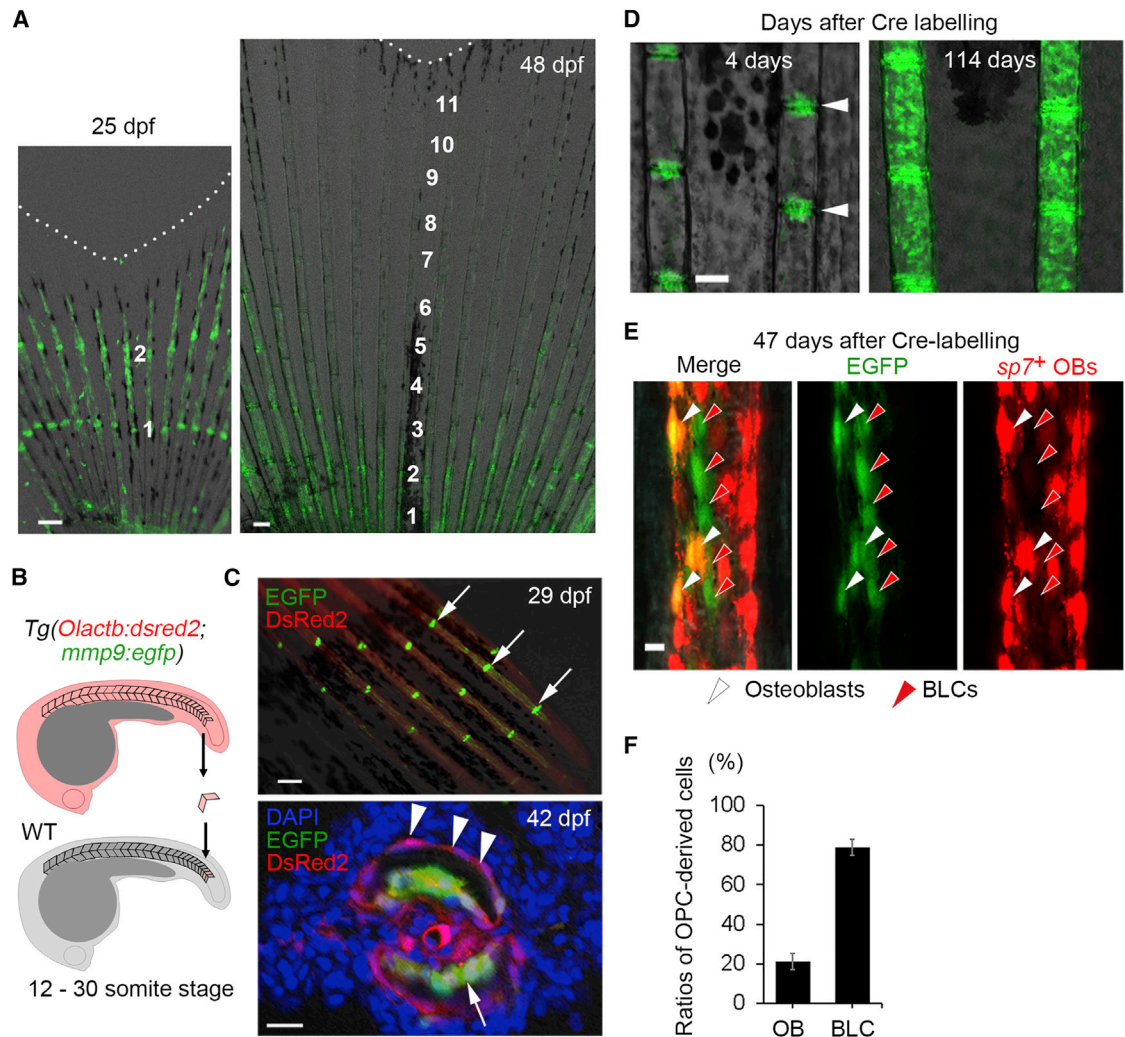
Figure 4. Origin and Development of OPCs and Their Role in Osteoblast Maintenance

(A) Tracing of early OPCs labeled at 25 dpf. Progenies of Cre-labeled OPCs contributed to neither newly added OPCs nor osteoblasts in the distal regions (n = 9 of 9 fish), suggesting that OPCs are produced by non-OPC precursor cells. Numbers denote fin ray joints. Scale bars, 100 μm.

(B) A diagram of somite transplantation. Somites that ubiquitously expressed DsRed2 were taken from double Tg(mmp9:egfp; Olactb:loxP-dsred2-loxP-egfp) and transplanted into WT.

(C) Differentiation of somite-derived cells into OPCs in fin ray joints. Upper panel: whole-mount view of the fin; lower panel: a section through the fin ray joint. As in a previous study in medaka fish (Shimada et al., 2013), the somite-derived cells (DsRed2$^+$) contributed to mesenchymal cells and osteoblasts in fin rays. Significantly, the somite-derived cells also differentiated into the EGFP$^+$ joint OPCs in 5 of 5 successful transplantations, strongly suggesting that OPCs are derived from the somites. Arrows, OPCs; arrowheads, osteoblasts or BLCs derived from transplanted somite. Nuclei, DAPI. Scale bars, 100 μm (upper panel) and 10 μm (lower panel).

(D) Fluorescent stereomicroscope images of EGFP$^+$ cells at 4 days and 114 days after Cre-loxP recombination. Joint OPCs (arrowheads) were labeled by Cre recombination at 4 months of age. Labeled OPCs gradually differentiated into cells on the surfaces of fin rays. Scale bar, 100 μm.

(E) Confocal z-stack image of progenies of Cre-labeled joint OPCs in adult fish that also carry the sp7:mcherry transgene. Progenies of OPCs in uninjured adult fins contain both mCherry$^+$ (sp7-expressing) osteoblasts (white arrowheads) and mCherry$^-$ BLCs (red arrowheads), which distribute in the non-joint region. Scale bar, 10 μm.

(F) Ratios of OPC-derived osteoblasts (OBs) and BLCs in non-regenerating fin rays. Cells were counted in a fin ray segment of the central fin region in each fish. Error bars indicate mean ± SEM (n = 5 fish).

Our study highlighted that OPCs are a reserved source of osteoblasts for bone regeneration and maintenance in adult zebrafish. Whereas it is well known that osteoblasts develop from somite sclerotomes and neural crest cells during vertebrate development (Hall, 2015a, 2015b), it has been assumed that mesenchymal stem cells in the bone marrow and their committed progenitor cells, OPCs, are the source of osteoblasts in post-developmental stages in mammals (Aubin, 2008). However, the identity of mammalian OPCs and their link to embryonic origins are not well understood. Our findings revealed the identity of OPCs and clarified that osteoblasts in the adult stage originate from the somites, as is the case with embryonic osteoblasts.

CellPress

A cascade of progenitor cell pools, such as OPCs and their mesenchymal precursors, may reinforce and ensure robust skeletal regeneration. Additionally it has been thought that Mmp9, a secreted metalloprotease that degrades the cartilage matrix, facilitates remodeling and deposition of bone matrix (Colnot et al., 2003). However, our finding that Mmp9 marks bone progenitors might suggest that Mmp9 has additional roles in these progenitors beyond extracellular matrix (ECM) remodeling, or that ECM remodeling is important for OPC function. Considering the higher bone regeneration potential in zebrafish, OPCs will be a potential target for enhancing bone regeneration in mammals.

STAR★METHODS

Detailed methods are provided in the online version of this paper and include the following:

- KEY RESOURCES TABLE
- CONTACT FOR REAGENT AND RESOURCE SHARING
- EXPERIMENTAL MODEL AND SUBJECT DETAILS
  - Zebrafish
- METHOD DETAILS
  - Transgenic Zebrafish
  - Cre-*loxP* Recombination and Lineage Tracing
  - Time-Lapse Recording of Joint Cell Migration
  - Cell Ablation
  - Whole-Mount *In Situ* Hybridization
  - Histological Methods
  - Staining of Calcified Bone and Quantification
  - Somite Transplantation
  - Blastema Transplantation
- QUANTIFICATION AND STATISTICAL ANALYSIS

SUPPLEMENTAL INFORMATION

Supplemental Information includes four figures and one table and can be found with this article online at https://doi.org/10.1016/j.devcel.2017.10.015.

REFERENCES

Akimenko, M.A., Johnson, S.L., Westerfield, M., and Ekker, M. (1995). Differential induction of four msx homeobox genes during fin development and regeneration in zebrafish. Development *121*, 347–357.

Aubin, J.E. (2008). Mesenchymal stem cells and osteoblast differentiation. In Principles of Bone Biology, J.P. Bilezikian, L.G. Raisz, and T.J. Martin, eds. (Academic Press), pp. 85–107.

Brockes, J.P., and Kumar, A. (2005). Appendage regeneration in adult vertebrates and implications for regenerative medicine. Science *310*, 1919–1923.

Bussmann, J., and Schulte-Merker, S. (2011). Rapid BAC selection for tol2-mediated transgenesis in zebrafish. Development *138*, 4327–4332.

Colnot, C., Thompson, Z., Miclau, T., Werb, Z., and Helms, J.A. (2003). Altered fracture repair in the absence of MMP9. Development *130*, 4123–4133.

Dallas, S.L., Prideaux, M., and Bonewald, L.F. (2013). The osteocyte: an endocrine cell… and more. Endocr. Rev. *34*, 658–690.

Grohmann, M., Paulmann, N., Fleischhauer, S., Vowinckel, J., Priller, J., and Walther, D.J. (2009). A mammalianized synthetic nitroreductase gene for high-level expression. BMC Cancer *9*, 301.

Hall, B.K. (2015a). Skeletal Origins: neural crest cells. In Bones and Cartilage: Developmental and Evolutionary Skeletal Biology (Academic Press), pp. 281–298.

Hall, B.K. (2015b). Skeletal origins: somitic mesoderm, vertebrae, pectral and pelvic girdles. In Bones and Cartilage: Developmental and Evolutionary Skeletal Biology (Academic Press), pp. 261–279.

Hans, S., Freudenreich, D., Geffarth, M., Kaslin, J., Machate, A., and Brand, M. (2011). Generation of a non-leaky heat shock-inducible Cre line for conditional Cre/lox strategies in zebrafish. Dev. Dyn. *240*, 108–115.

Johnson, S.L., and Weston, J.A. (1995). Temperature-sensitive mutations that cause stage-specific defects in zebrafish fin regeneration. Genetics *141*, 1583–1595.

Kawakami, A. (2010). Stem cell system in tissue regeneration in fish. Dev. Growth Differ. *52*, 77–87.

Knopf, F., Hammond, C., Chekuru, A., Kurth, T., Hans, S., Weber, C.W., Mahatma, G., Fisher, S., Brand, M., Schulte-Merker, S., et al. (2011). Bone regenerates via dedifferentiation of osteoblasts in the zebrafish fin. Dev. Cell *20*, 713–724.

Kragl, M., Knapp, D., Nacu, E., Khattak, S., Maden, M., Epperlein, H.H., and Tanaka, E.M. (2009). Cells keep a memory of their tissue origin during axolotl limb regeneration. Nature *460*, 60–65.

Li, N., Felber, K., Elks, P., Croucher, P., and Roehl, H.H. (2009). Tracking gene expression during zebrafish osteoblast differentiation. Dev. Dyn. *238*, 459–466.

Matic, I., Matthews, B.G., Wang, X., Dyment, N.A., Worthley, D.L., Rowe, D.W., Grcevic, D., and Kalajzic, I. (2016). Quiescent bone lining cells are a major source of osteoblasts during adulthood. Stem Cells *34*, 2930–2942.

Narayanan, K., and Chen, Q. (2011). Bacterial artificial chromosome mutagenesis using recombineering. J. Biomed. Biotechnol. *2011*, 971296.

Pisharath, H., Rhee, J.M., Swanson, M.A., Leach, S.D., and Parsons, M.J. (2007). Targeted ablation of beta cells in the embryonic zebrafish pancreas using E. coli nitroreductase. Mech. Dev. *124*, 218–229.

Poss, K.D. (2010). Advances in understanding tissue regenerative capacity and mechanisms in animals. Nat. Rev. Genet. *11*, 710–722.

Renn, J., and Winkler, C. (2009). Osterix-mCherry transgenic medaka for in vivo imaging of bone formation. Dev. Dyn. *238*, 241–248.

Sharif, F., de Bakker, M.A.G., and Richardson, M.K. (2014). Osteoclast-like cells in early zebrafish embryos. Cell J. *16*, 211–224.

Shibata, E., Ando, K., and Kawakami, A. (2017). Transplantation of mesenchymal cells including the blastema in regenerating zebrafish fin. bio-protocol *7*, e2109.

Shibata, E., Yokota, Y., Horita, N., Kudo, A., Abe, G., Kawakami, K., and Kawakami, A. (2016). Fgf signalling controls diverse aspects of fin regeneration. Development *143*, 2920–2929.

Shimada, A., Kawanishi, T., Kaneko, T., Yoshihara, H., Yano, T., Inohaya, K., Kinoshita, M., Kamei, Y., Tamura, K., and Takeda, H. (2013). Trunk exoskeleton in teleosts is mesodermal in origin. Nat. Commun. *4*, 1639.

Singh, S.P., Holdway, J.E., and Poss, K.D. (2012). Regeneration of amputated zebrafish fin rays from de novo osteoblasts. Dev. Cell *22*, 879–886.

Stewart, S., and Stankunas, K. (2012). Limited dedifferentiation provides replacement tissue during zebrafish fin regeneration. Dev. Biol. *365*, 339–349.

Sousa, S., Afonso, N., Bensimon-Brito, A., Fonseca, M., Simões, M., Leon, J., Roehl, H., Cancela, M.L., and Jacinto, A. (2011). Differentiated skeletal cells contribute to blastema formation during zebrafish fin regeneration. Development *138*, 3897–3905.

Suster, M.L., Abe, G., Schouw, A., and Kawakami, K. (2011). Transposon-mediated BAC transgenesis in zebrafish. Nat. Protoc. *6*, 1998–2021.

Takeyama, K., Chatani, M., Takano, Y., and Kudo, A. (2014). In-vivo imaging of the fracture healing in medaka revealed two types of osteoclasts before and after the callus formation by osteoblasts. Dev. Biol. *394*, 292–304.

Tanaka, E.M., and Reddien, P.W. (2011). The cellular basis for animal regeneration. Dev. Cell *21*, 172–185.

Tu, S., and Johnson, S.L. (2011). Fate restriction in the growing and regenerating zebrafish fin. Dev. Cell *20*, 725–732.

Yoshinari, N., and Kawakami, A. (2011). Mature and juvenile tissue models of regeneration in small fish species. Biol. Bull. *221*, 62–78.

Yoshinari, N., Ando, K., Kudo, A., Kinoshita, M., and Kawakami, A. (2012). Colored medaka and zebrafish: transgenics with ubiquitous and strong transgene expression driven by the medaka β-actin promoter. Dev. Growth Differ. *54*, 818–828.

Yoshinari, N., Ishida, T., Kudo, A., and Kawakami, A. (2009). Gene expression and functional analysis of zebrafish larval fin fold regeneration. Dev. Biol. *325*, 71–81.

CellPress

STAR★METHODS

KEY RESOURCES TABLE

REAGENT or RESOURCE	SOURCE	IDENTIFIER
Antibodies		
Rabbit polyclonal anti-OSX (A-13)	Santa Cruz Biotechnology	Cat#: sc-22536-R; RRID: AB_831618
Mouse monoclonal anti-RUNX2 (27-K)	Santa Cruz Biotechnology	Cat#:sc-101145; RRID: AB_1128251
Mouse monoclonal zns-5 antibody	Developmental Studies Hybridoma Bank	Cat#: zns-5; RRID: AB_10013796
Chemicals		
4-OH Tamoxifen (TAM)	Sigma Aldrich	Cat#:H7904
Tricaine	Sigma Aldrich	Cat#:A5040
Metronidazole (Mtz)	Tokyo Chemical Industry	Cat#:M0924
Alizarin Complexone	DOJINDO	Cat#: A006
Alizarin red S	Nacalai tesque	Cat#: 01303-52
Recombinant DNA		
BAC (mmp9:egfp)	This paper	N/A
BAC (mmp9:egfp-nfsB)	This paper	N/A
BAC (mmp9:creERt2; cryaa:egfp)	This paper	N/A
pTol2 (Olactb:loxp-bfp-loxp-egfp)	This paper	N/A
pTol2 (sp7:mcherry)	This paper	N/A
Experimental Models: Organisms/Strains		
Zebrafish: *Tg(mmp9:egfp)*	This paper	N/A
Zebrafish: *Tg(mmp9:egfp-nfsB)*	This paper	N/A
Zebrafish: *Tg(mmp9:creERt2)*	This paper	N/A
Zebrafish: *Tg(Olactb:loxP-dsred2-loxP-egfp)*: *tyt21Tg*	Yoshinari et al., 2009	ZFIN: ZDB-ALT-130220-1
Zebrafish: *Tg(Olactb:loxp-bfp-loxp-egfp)*	This paper	N/A
Zebrafish: *Tg(sp7:mCherry)*	This paper	N/A
Softwares		
LAS AF ver3.1	Leica	Leica-microsystems.com
Zen 2 ver10.0	Carl Zeiss	www.zeiss.com
FV10 ASW ver4.2	Olympus	www.olympus-lifescience.com
ImageJ ver1.49	NIH	imagej.nih.gov/ij/

CONTACT FOR REAGENT AND RESOURCE SHARING

Further information and requests for resources and reagents should be directed to and will be fulfilled by the Lead Contact, Atsushi Kawakami (atkawaka@bio.titech.ac.jp).

EXPERIMENTAL MODEL AND SUBJECT DETAILS

Zebrafish

WT zebrafish (*Danio rerio*) strain, which is originally derived from Tubingen strain and maintained in our facility for more than 10 years by inbreeding, and all transgenic lines were kept in a recirculating water system in a 14-hr day/10-hr night photoperiod at 28.5°C. Adults between 3 and 12 months of both sexes were used. Transgenic lines used in this study were described below. All transgenic strains were analyzed as hemizygotes. Animal procedures were approved by Animal Care and Use Committee at the Tokyo Institute of Technology. All surgical procedures were performed under anesthesia with 0.002% tricaine (3-aminobenzoic acid ethyl ester) (Sigma-Aldrich, St. Louis, MO), and every effort was made to minimize suffering. The bone fracture assay was performed according to the described procedure (Takeyama et al., 2014). To induce scale regeneration, approximately 10 scales were removed from the left trunk region of the fish using forceps.

METHOD DETAILS

Transgenic Zebrafish

For generating *mmp9 Tgs*, the BAC DNA was modified according to the BAC recombineering method (Narayanan and Chen, 2011; Suster et al., 2011; Bussmann and Schulte-Merker, 2011). The respective gene cassettes of *egfp*, *creERt2* (Hans et al., 2011) or *egfp-nfsB* (Grohmann et al., 2009) that also carry the polyadenylation sequence and kanamycin resistance gene were inserted at the translational initiation codon of *mmp9* in the BAC clone, CH211-269M15, by homologous recombination (Figure S1A; Table S1). The *nfsB* is the human codon-optimized version of the *Escherichia coli* gene encoding nitroreductase (Grohmann et al., 2009). To facilitate the identification of transgenic fish, *egfp* under the control of crystalline alpha A promoter, was introduced into the iTol2 cassette that carries the ampicillin resistance gene (Suster et al., 2011), and the modified iTol2 cassette was introduced into the *mmp9* BAC clone. The engineered BAC DNAs were purified by using the PureLink HiPure Plasmid Midiprep Kit (Invitrogen) and injected into one-cell-stage zebrafish embryos at 125 ng/μl with 25 ng/μl transposase mRNA. By crossing the founder fish to each other or with WT fish, we screened for EGFP expression in F1 offspring and identified 2 and 3 fish lines of *egfp* and *egfp-nfsB* lines, respectively. As these F1 fish had an indistinguishable EGFP expression, each one of respective lines were selected and established as *Tg* lines. The *Tg(mmp9:creERt2)* was firstly screened for the EGFP expression in the lens and then tested for the Cre recombination by treating them with TAM in adult fish. We identified 8 Cre lines with the lens EGFP expression, and the one that showed highest recombination frequency was selected and established as the *Tg* line.

The *Tg(sp7:mcherry)* was generated in our facility. The *sp7* promoter and the *mcherry* coding sequence were cloned into the *pTol2(ef1a:egfp)* vector using the SfiI and AgeI sites and AgeI and ClaI sites, respectively. The plasmid DNAs were injected into one-cell-stage embryos at 25 ng/μl along with 25 ng/μl transposase mRNA.

Cre-*loxP* Recombination and Lineage Tracing

The *Tg* strain carrying the *mmp9:creERt2* was crossed with the *Tg(Olactb:loxP-dsred2-loxP-egfp)* (Yoshinari et al., 2012) or *Tg(Olactb:loxP-bfp-loxP-egfp)* to generate the double *Tg* line. Cre-*loxP* recombination was induced by treating the double *Tg* with TAM in fish water (with 0.3% artificial sea salt and 0.0001% methylene blue). For most experiments, the recombination was induced with 5 μM TAM for 12 hours. The treated fish were kept in an aquarium at least 2 days, and fins were amputated 3 days later. For labeling *mmp9+* cells during an early stage of fin growth (Figure 4A), TAM treatment was performed for 4 days to maximize the number of labeled cells.

Time-Lapse Recording of Joint Cell Migration

For live imaging of the *Tgs*, fish were anaesthetized with 0.002% tricaine. Fins were embedded in 1.5% low melting point agarose gel and observed under the 60× water-immersion objective lens of a confocal laser scanning microscope (FV-1000, Olympus). Images were taken every 2-6 hrs intervals.

Cell Ablation

The nitroreductase-mediated cell ablation was performed by treating the *Tg(mmp9:egfp-nfsB)* with 5 mM Mtz (Sigma-Aldrich or Tokyo Chemical Industry) in fish water (approximately 100 ml solution per adult fish). The fish container was kept in dark at 28.5°C, and fish water containing Mtz was daily changed with freshly prepared one. On every instance of water change, the fish were transferred to fresh aquarium water for 3-6 hours and fed brine shrimp.

For long-term cell ablation (Figures S4E–S4N), the Mtz treatment was performed for 12-18 hours every 2 days for fish in fin growing stage (20 to 28 dpf) and every 4 days for adult fish above 3 months of age. EGFP fluorescence was checked immediately before each Mtz treatment, but the recovery of EGFP+ cells was rarely observed (Figures S4E and S4J). Fins were fixed for analysis immediately following the last Mtz treatment.

Whole-Mount *In Situ* Hybridization

Whole-mount *in situ* hybridization (ISH) was performed according to the standard protocol. For RNA probe generation, a region of the *mmp9* coding sequence was amplified by PCR using the following primers. *mmp9* fw, 5'-GATGCCCTGATGTATCCCAT-3'; *mmp9* rv, 5'-ACTTCACATAACCGACTCGG-3'. The PCR product was cloned into the pCR4 vector (Clontech). The *egfp* probe was synthesized from the pCS2-*egfp*, which harbors the *egfp* sequence in the pCS2 vector.

Histological Methods

Antibody staining was performed as described previously (Shibata et al., 2016). Zns5 antibody was used at 1:100 dilution of the hybridoma supernatant (Developmental Studies Hybridoma Bank), the Sp7 antibody at 20 ng/ml (A-13, Santa Cruz Biotechnology) and the Runx2 antibody at 100 ng/ml (27-K, Santa Cruz Biotechnology). Nuclei were counterstained with 4′,6-diamidino-2-phenyl-indole (DAPI) (0.1 μg/ml in PBSTx; Invitrogen) or TO-PRO-3 (1 μg/ml in PBSTx; Invitrogen). TRAP staining was performed as described (Sharif et al., 2014). Cell proliferation was detected by EdU labeling using the Click-iT EdU Imaging Kit (Life Technologies). Fish were incubated in a solution containing 50 μM EdU in fish water for 24 hours at 28.5°C.

Staining of Calcified Bone and Quantification

Fins were fixed with 4% PFA in PBS. Samples were incubated with 50% ethanol for 30 min and stained with 0.01% Alizarin red S (A5533, Sigma-Aldrich) in 0.5% potassium hydroxide overnight. The fins were bleached for 20 min at room temperature using a freshly prepared solution containing 1.5% hydrogen peroxide and 1% potassium hydroxide. Alizarin complexone (ALC) (Dojin Chemical) was used at 0.005% in aquarium water for 12 hours.

Fin images were captured under the same conditions and analyzed using ImageJ 1.49 to quantify mineralization in the regenerated fin. Mineralized areas were measured by applying a color threshold (Red-Green-Blue color model) to select only the areas appearing in red. Measurements in terms of pixels were converted into unit of area.

Somite Transplantation

Somite transplantation was performed according to the previously described method in medaka fish (Shimada et al., 2013). The double *Tg(mmp9:egfp; Olactb:loxP-dsred2-loxP-egfp)* was used as the donor. The transplanted somites were fated to become dorsal or anal fins by operation at early stages and the tail fin by operation at a later stage (approximately 30-somite stage). The operated embryos were incubated at 28.5°C, and the successfully transplanted ones were raised to adulthood.

Blastema Transplantation

Blastema transplantation was performed as previously described (Yoshinari et al., 2012; Shibata et al., 2016, 2017). In this study, whole blastema region distal to amputation site was dissected at 2 dpa from the double *Tg(mmp9:egfp; Olactb:loxP-dsred2-loxP-egfp)* as a donor and transplanted into the host blastema region of *Tg(mmp9:egfp-nfsB)* at 2 dpa.

QUANTIFICATION AND STATISTICAL ANALYSIS

Clutchmates were randomized into different treatment groups for each experiment. No animal or sample was excluded from the analysis unless the animal died during the procedure. All experiments were performed with at least 2 biological replicates, using the appropriate number of samples for each replicate. Sample sizes were chosen based on previous publications and experiment types and are indicated in each figure legend. For ISH analysis of expression patterns, at least six fish were examined. For quantification of mineralized areas, fin images were captured under the same conditions and analyzed using the NIH ImageJ 1.49 to quantify mineralization in the regenerated fin. Mineralized areas were measured by applying a color threshold (Red-Green-Blue color model) to select only the areas appearing in red. Measurements in terms of pixels were converted into unit of area. Statistical analyses were performed using Microsoft Excel 2013. All statistical values are displayed as mean ± standard error of the mean. Sample sizes, statistical tests and P values are indicated in the figures or the legends. Student's t-tests (two-tailed) were applied when normality and equal variance tests were passed.